International Journal of Hydrogen Energy 80 (2024) 394–405

Contents lists available at ScienceDirect

International Journal of Hydrogen Energy

journal homepage: www.elsevier.com/locate/he

On fluctuations in velocity fields during convective mass transfer in hydrogen generation through water electrolysis

Jeferson Diehl de Oliveira [a,*], Elaine Maria Cardoso [b,c], Reinaldo Rodrigues de Souza [d], Jacqueline Biancon Copetti [e], Lina Maria Varón [a], José Roberto Simões Moreira [a]

[a] SISEA - Renewable and Alternative Energy Systems Laboratory, Polytechnic School of the University of São Paulo, Brazil
[b] UNESP - São Paulo State University, School of Engineering, Av. Brasil, 56, Ilha Solteira, SP, 15385-000, Brazil
[c] UNESP - São Paulo State University, School of Engineering, São João da Boa Vista, Brazil
[d] IN+ Center for Innovation, Technology and Policy Research, Instituto Superior Técnico, University of Lisboa, Av. Rovisco Pais, Lisboa, 1049-001, Portugal
[e] Mechanical Engineering Graduate Program, LETEF, Laboratory of Thermal and Fluid Dynamic Studies, University of Vale do Rio dos Sinos, São Leopoldo, 93022-750 RS, Brazil

ARTICLE INFO

Handling Editor: Z Sun

Keywords:
Hydrogen generation
Renewable energy
Electrolysis
Velocity field

ABSTRACT

This study investigates the hydrodynamic behavior and mass transfer performance in water electrolysis within an alkaline solution (30% wt KOH). By using a glass electrolyzer with vertical stainless steel 304 electrodes spaced 20 mm apart, the research employs an optical flow method to analyze the velocity field of hydrogen bubbles. Image sequences captured by a CCD camera with a pixel resolution of 67.2 μm facilitate this analysis. The study focuses on the effect of current density, ranging from 33 to 650 A/m^2. Experimental results demonstrate that the velocity distribution in most areas of the electrolyzer is primarily influenced by two asymmetric flow patterns caused by the buoyancy of hydrogen and oxygen bubble layers. Regions with lower depths exhibit increased velocity and vorticity fields, resulting in greater motion within the electrolyte. Conversely, at higher current densities, the average velocity decreases due to the expansion of dynamic areas. These complex flow structures significantly affect bubble dynamics, causing velocity fluctuations between the electrodes. The findings offer valuable insights into hydrogen bubbles' dynamics and transport phenomena within the electrolyzer, enhancing the understanding of bubble behavior in alkaline water electrolysis.

Nomenclature

g	Normalized Image Intensity [−]
J	Current density [A/m^2]
LDV	Laser Doppler Velocimetry
PIV	Particle Image Velocimetry
PLIF	Planar Laser-Induced Fluorescence
PTV	Particle Tracking Velocimetry
u_x	Horizontal velocity [mm/s]
u_y	Vertical velocity [mm/s]
U	Total velocity [mm/s]
x	Horizontal Direction
y	Vertical Direction
Greek Abbreviation	
Δh	Pixel Size [μm]
Δt	Time interval [s]
∇	Nabla Operator
λ	Lagrange multiplier

1. Introduction

In recent years, various issues concerning energy generation and transformation issues have garnered significant attention, mainly due to their environmental consequences. This growing concern has highlighted the need to develop cleaner and more sustainable energy sources. Consequently, green hydrogen, produced through electrolysis, has emerged as an appealing solution owing to its minimal environmental impact and high calorific value [1,2]. However, numerous challenges persist in enhancing hydrogen generation efficiency through electrolysis, [1].

Many researchers have also focused studies on the modeling hydrogen generation based on both theory and experimental observation [3–6], including the effect of pressure [7], temperature [8,9], volume of hydrogen generated [10]. During the process of electrolysis of water, electrons flow through the anode to the cathode, where hydrogen

* Corresponding author.
E-mail address: jef.diehl@usp.br (J. Diehl de Oliveira).

https://doi.org/10.1016/j.ijhydene.2024.07.141
Received 9 April 2024; Received in revised form 2 July 2024; Accepted 10 July 2024
Available online 16 July 2024

ions incorporate them to form hydrogen gas. In this way, the dissolved gas accumulates until it reaches a critical condition of supersaturated concentration at the electrode surface, initiating bubble nucleation [11, 12]. By starting from the nucleation site, a gas bubble begins to develop, potentially obstructing other sites. This obstacle hampers the interaction between ions and the surface, consequently impeding the generation of fresh hydrogen bubbles. Only after the bubble departure is the surface re-wetting by the electrolyte resume [7].

Avci and Toklu [13] studied flow analysis of bubbles during water electrolysis using vertical electrodes. The authors investigated the effect of void fraction, the gap between electrodes, on bubble diameter and bubble velocity. As a result, they developed a parametric function of acceleration velocity for hydrogen gas after production. Also, they observed that during the separation of hydrogen gas from the electrode, the velocity of the hydrogen gas bubble under the influence of drag and buoyancy forces also depends on the drift coefficient.

An experimental investigation was performed by Ref. [14] focusing on the density distributions of bubble sizes detached from the nickel cylindrical wire electrode. In their study, a system with a high-speed video camera was developed, achieving *in-situ* observation of bubble generation on an electrode surface. Their investigation tested electrodes for different current densities, including cylindrical, rectangular and Raney-nickel wires. Their results show that bubble size depends on electrode geometry and current density.

Hydrodynamic parameters on cirtical current density were investigated by Ref. [15], including void fraction, and mass flux during eletrolyis. According to the results, the mass flux increase delayed the film's formation, consequently elevating the critical current density, irrespective of the channel's inclination or the inlet void fraction. Moreover, the increase in void fraction leads to the development of flow patterns, ranging from dispersed bubbles to slug flow, depending on parameters such as inlet void fraction and electrode inclination.

More recently [16], performed an experimental study to investigate the influence of temperature on the growth of H_2 bubbles under ultrasonic conditions. As a result, temperature's effect on the frequency of bubble nucleation is tied to the Gibbs free energy needed for the electrolytic reaction, the surface tension coefficient, and the liquid's molecular number density. Both the growth radius and growth rate of hydrogen bubbles follow a one-third power relationship with temperature. The surface tension coefficient and contact angle primarily influence temperature's impact on the bubble escape radius. Additionally, the alternating positive and negative sound pressure generated by ultrasound will hasten the detachment of hydrogen bubbles.

Convection can result from natural buoyancy or forced convection, while diffusion arises from concentration gradients of reactants and products at the electrode-electrolyte interface and in the bulk. As a result, substantial efforts have been dedicated to investigating the dynamic fluid behavior of the gas phase. This includes studying the effects of convection, velocity profiles, bubble initiation, and the influence of parameters such as current density, electrode gap, concentration, temperature, and pressure. Numerous experimental investigations have been reported in the literature that delve into various aspects of water electrolysis, particularly focusing on bubbles' key fluid dynamic characteristics. To this end, various experimental techniques have been employed to visualize velocity fields and bubble growth. These techniques include Particle Image Velocimetry (PIV), Laser Doppler Velocimetry (LDV), Planar Laser-Induced Fluorescence (PLIF), and Particle Tracking Velocimetry (PTV), among others.

Abdelouahed et al. [17] studied the hydrodynamics of gas bubbles during water electrolysis using NaOH as the electrolyte. The authors investigated the distributions of bubble velocities and void fractions within the anode-to-cathode space, exploring the effects of the anode gap, current density and cell inclination on the hydrodynamics of the gas phase. Zhu et al. [18] investigated the hydrodynamics behavior and mass transfer performance in water electrolysis processes, utilizing two different containers and electrode configurations under varying current densities. The authors employed the PIV method to obtain the velocity field data. According to their results, the mean vertical velocity increases with rising current density, and the natural convection is enhanced with Joule heat generation at higher current densities.

Babu and Das [19] conducted a study investigating the instantaneous velocity and concentration fields using PIV and PLIF techniques. Their research aimed to explore the mass transfer processes occurring at the electrode-electrolyte interface of a water-splitting electrochemical cell. The authors examined the impact of cell voltage, electrode orientation, and the concentration gradient resulting from reactant depletion and product formation at the interface on the mass transfer rate. Their experiments encompassed various current densities and electrode orientations, and the observations revealed that reactant depletion and product formation at the anode interface led to buoyancy effects, causing natural convection even at low current densities.

Chen et al. [20] employed PIV to investigate the impact of flow characteristics on electrochemical water softening. They analyzed the flow fields near vertical plate electrodes within a bench-scale electrolysis cell and measured the hardness drop values under various process conditions. The study revealed that increasing the current density or decreasing the electrode spacing can effectively enhance the average flow velocity within the electrode gap. The velocity of bubble-driven convection resulting from bubble floating is observed to be 5–9 times higher than that of natural convection caused by bubble aggregation. Increasing the current density has a notable effect on enhancing both bubble-driven convection and natural convection velocities. However, excessive current density can accumulate bubbles on the water and electrode surfaces. This accumulation of bubbles disrupts the surrounding liquid and reduces the velocity of liquid passing through the bubbles.

On the other hand, studies have been developed to investigate the fluid dynamic behavior of bubbles using image capture methods. In their work, Chandran et al. [21] analyzed the bubble size distribution of hydrogen in electrolysis using sodium chloride and horizontal electrodes. Through image processing, the authors established the relationship between the number of bubbles and their respective diameters.

An experimental investigation on bubble shape observation was performed by Ref. [22] during electrolysis using a laser-based shadow imaging system and an online vapor monitoring system. The authors modeled bubble dynamics and vapor transfer kinetics considering parameters such as bubble diameter, velocity and trajectories under different operation conditions.

Yang et al. [23] used a visualization technique with a high-speed and microscale visualization system to observe the bubble generation site and growth rate that can be used to quantify the electrochemical reaction site and intensity for both the oxygen and hydrogen evolution reactions. As part of their result, they observed the smaller bubble detachment diameter and the increased number of reaction sites with 100 nm AuNL reduce the mass transport overpotential in water electrolysis. This explains the low-frequency arc in the EIS and the absence of curvature in the polarization curves when using 100 nm AuNL.

Li et al. [24] conducted a study utilizing a high-speed visualization system to investigate the behavior of oxygen bubbles and their multiphase evolutions in the anode side of proton exchange membrane electrolysis cells (PEMECs) equipped with liquid gas diffusion layers (LGDLs) made of titanium (Ti) felt. Different two-phase flow patterns have been visually observed and analyzed under different operating conditions, specifically focusing on oxygen bubbles' ultra-fast and micro-scale detachment process. The authors observed that different flow velocities had an impact on the diameter of bubble detachment, suggesting a relationship with detachment time. They found that increasing the flow velocity could potentially lead to an increased frequency of bubble detachment during the bubble detachment process.

In parallel with experimental investigations, various authors have made significant efforts in numerical studies related to bubble growth, dynamics, and velocity field during electrolysis under different

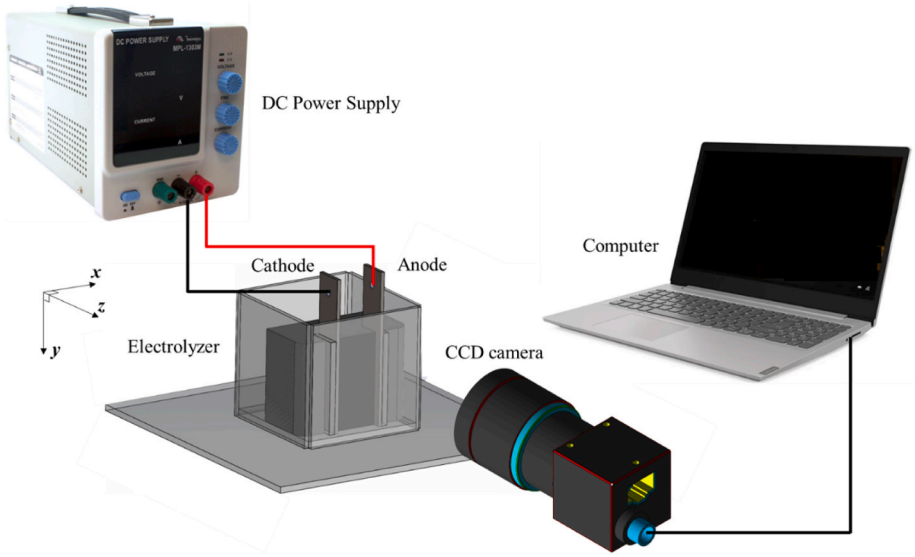

Fig. 1. Experimental apparatus (without high-brightness diodes).

conditions. Torri et al. [25] investigated used three-dimensional coupled numerical simulations of two-phase flow and electrochemical phenomena in alkaline water electrolysis to clarify how microscale bubbles affect ion transport and cell overpotential. They focused on the effect of rising bubbles and bubble atomization on the overpotential. They discovered that the cell overpotential was reduced by the rising bubbles, with this reduction becoming more pronounced due to bubble atomization. The rising bubbles lowered the activation overpotential at the anode because the flow induced by the bubbles improves ion transport to the anode and boosts the concentration of hydroxide ions at the anode surface. They explained that bubble atomization further enhanced this reduction since smaller bubbles can get closer to the anode than larger ones, thereby increasing the convective ion flux to the anode surface.

More recently, Sarma et al. [26] numerically investigated bubble hydrodynamics in water splitting, considering the effect of electrolyte inflow velocity and electrode morphology. Their study analyzed the flow fields of bubbles near the electrode and bubble detachment from the electrode surface. Babay et al. [27] developed a 2D two-phase electrochemistry-transport model using an inhomogeneous Euler-Euler mixture modeling approach. They presented multidimensional contours of hydrogen and oxygen volume fractions to illustrate electrochemical reactions and two-phase transport phenomena. The authors reported that bubble nucleation and two-phase flow in the large-scale cell significantly increased overpotentials. The hydrogen volume fraction was higher than that of oxygen due to lower oversaturation. More severe bubble blockage was observed at the negative electrode because of the differences in reaction stoichiometry.

An experimental and numerical study was conducted by Ref. [28] to investigate the dynamics of H_2 bubbles caused by convection during electrochemical water splitting. The results indicate that the fraction of the electrode surface covered by gas increases as the bubble diameter decreases. The same volume of gas can form either a few large bubbles or many small ones. The impact of current density is directly proportional to the volume of gas produced. According to Faraday's laws of electrolysis, this volume depends on the reaction stoichiometry and the applied current density. When large amounts of gas are generated, the bubbles tend to remain on the electrode surface longer.

Khalighi et al. [29] conducted a numerical investigation of a single stagnant and growing hydrogen bubble using an immersed boundary method implemented in an in-house code. To ensure the numerical accuracy of the method, the authors performed a grid refinement study and verified the global momentum and hydrogen mass balances. They also examined the effects of flow rate (Peclet number) and operating pressure. The results showed that both the bubble radius at a given time and the average concentration of hydrogen in the fluid domain decrease with increasing flow rate. Additionally, the current density at a given time increases with higher flow rates due to the reduced resistance caused by the smaller bubble radius.

As the electrochemical reaction progresses at the electrode/electrolyte interface, multiple concurrent mass transfer processes occur, as discussed earlier. Reactants are consumed, and products are generated at the interface, leading to concentration gradients forming, as Sahore et al. noted [30].

The flow field of electrolytes plays a critical role in governing ionic mass transfer, temperature distribution, bubble sizes, bubble detachment, and rising velocity. These factors, in turn, significantly impact current and potential distributions within the electrolysis reactor. This subject is complex and not yet fully understood, necessitating further research.

Despite the several efforts reported in the literature regarding the generation and transport of hydrogen during electrolysis, comprehending the dynamics of bubbles during this process remains a challenge. One of the most significant challenges is understanding the dynamics of the two-phase flow within the electrolyte, which arises due to the convection and vorticity zones generated by the turbulent nature of the phenomenon. Therefore, this study aims to analyze the velocity fields during alkaline water electrolysis using an optical flow method while considering the effects caused by current density and electrode gap.

1.1. Water electrolysis

In water electrolysis, reactants tend to migrate from the bulk to the interface, while the products move from the interface to the bulk. Simultaneously, alterations in the concentrations of reactants and products at the interface lead to changes in the thermophysical properties of the electrolyte, notably density, which, in turn, generates buoyant forces depending on their orientation relative to gravitational acceleration. The current experimental investigation is focused on the electrolysis of alkaline water. The electrolyte is a dilute solution of potassium hydroxide (KOH) solution, which disassociates into K^+ and OH^-. Thus, the oxygen gas evolves at the anode, while hydrogen gas is generated at the cathode according to the following electrochemical reaction at the anode:

$$2OH^- \rightarrow {}^1\!/\!_2 O_2(gas) + 2e^- + H_2O \quad (1)$$

Table 1
Experimental conditions during tests.

Properties and Parameters	Value/Range
Molar mass [mol/l]	5.34
Density of electrolyte [kg/m^3]	1237
Viscosity of electrolyte [kg/(m·s)]	0.001731
Current density [A/m^2]	33–650
Operating temperature [°C]	20

and at the cathode:

$$2H_2O + 2e^- \rightarrow H_2(gas) + 2OH^- \quad (2)$$

2. Experimental setup

An electrolyzer was developed to investigate the factors affecting hydrogen production during alkaline water electrolysis. Fig. 1 illustrates a schematic of the experimental setup, which consists of a transparent plexiglass cubic container with an 80 mm edge, vertical electrodes made of an iron-nickel alloy (20 mm × 60 mm) with a 20 mm separation between them, a DC power supply, a set of high-brightness diodes with adjustable intensity over electrodes, and a high-speed camera. Although this configuration is not typically encountered in industrial processes, it is often employed to better understand specific fundamental aspects of fluid dynamics of bubbles during electrolysis.

The electrodes were fixed to a polymeric support for the experimental tests to avoid image distortion, ensuring vertical alignment. This support has dimensions of 80 mm × 40 mm x 60 mm, with two slots on the front face to allocate the electrodes within the electrolytic cell. These slots have a width of 7 mm to accommodate the electrode along with the glass plate, a depth of 15 mm to fit 80% of the electrode (the submerged portion in the electrolyte), thus leaving a protrusion on the front face where H_2 bubbles will be produced, and a height of 60 mm, which represents the height of the support itself. The central face of the support is black to avoid reflections during image capture in the experiment.

In order to assess various electrolysis systems, it is essential to establish the correlation between practical parameters and the performance of different electrolyzers. Crucial parameters include reactor configurations and operational conditions. These parameters considered in this study are presented in Table 1.

2.1. Optical flow method

Optical flow methods offer a wide range of advantages in several applications, and over the last few years, significant advancements have

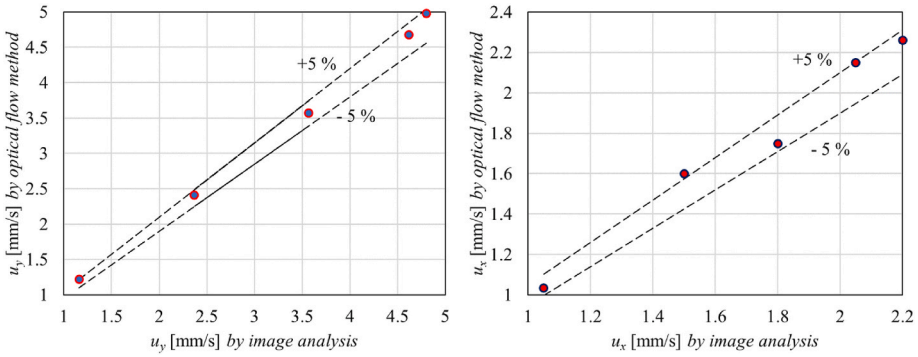

Fig. 2. Comparison between velocities obtained by optical flow method and by image analysis.

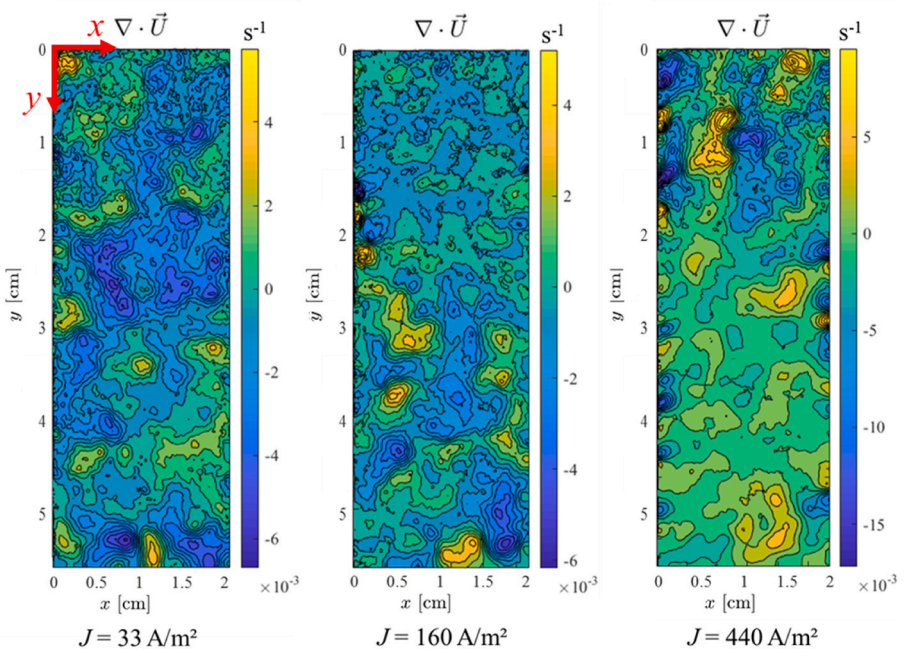

Fig. 3. Intensity of $\nabla \bullet \vec{U}$ for different conditions of J.

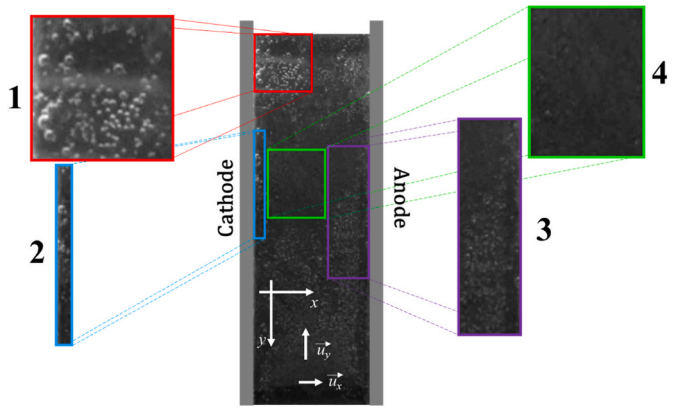

Fig. 4. Characteristic bubble distribution for $J = 260$ A/m^2.

been made in this field, including [31–35]. These methods excel in tracking and motion analysis, enabling the detection and segmentation of objects based on consistent motion patterns. Optical flow can operate in real-time, making it ideal for tasks requiring rapid video analysis, such as bubble generation. Its versatility and utility make optical flow an invaluable tool in the field of computer vision, aiding in the analysis and understanding of dynamic visual information. In this investigation, the optical flow employed is based on the approach developed by Ref. [36]. This method considers the optical flow equation for different flow visualizations, expressed in terms of image coordinates:

$$\frac{\partial g}{\partial t} + \nabla \cdot \left(g\vec{U}\right) - f(x,y,g) = 0 \tag{3}$$

where, g represents the normalized image intensity, which is proportional to the radiance received by the camera. The velocity in the image plane, denoted as $\vec{U} = (u_x, u_y)$, is referred to as the optical flow (*i.e.* pixel velocity), the operator $\nabla \equiv \partial/\partial x_i$ represents the spatial gradient while $f(x,y,g)$ corresponds to a boundary and diffusion term. The optical flow u is directly linked to the velocity averaged over the light path and is influenced by the field quantity Φ associated with the visualizing medium. Typically, the optical flow does not exhibit divergence-free characteristics, *i.e.*, $\nabla \bullet \vec{U} \neq 0$. But for special cases where $f(x,y,g) =$

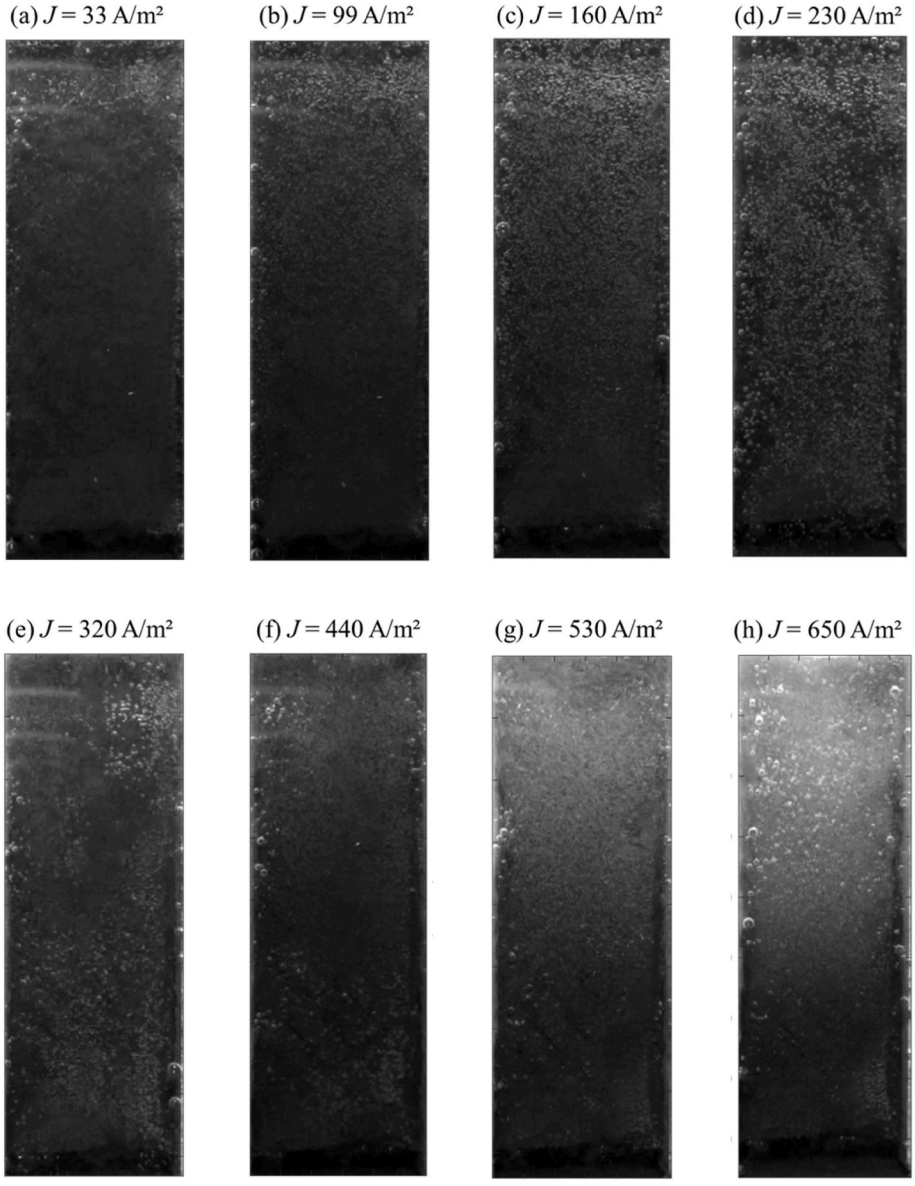

Fig. 5. Evolution of the void fraction with the increase in current density.

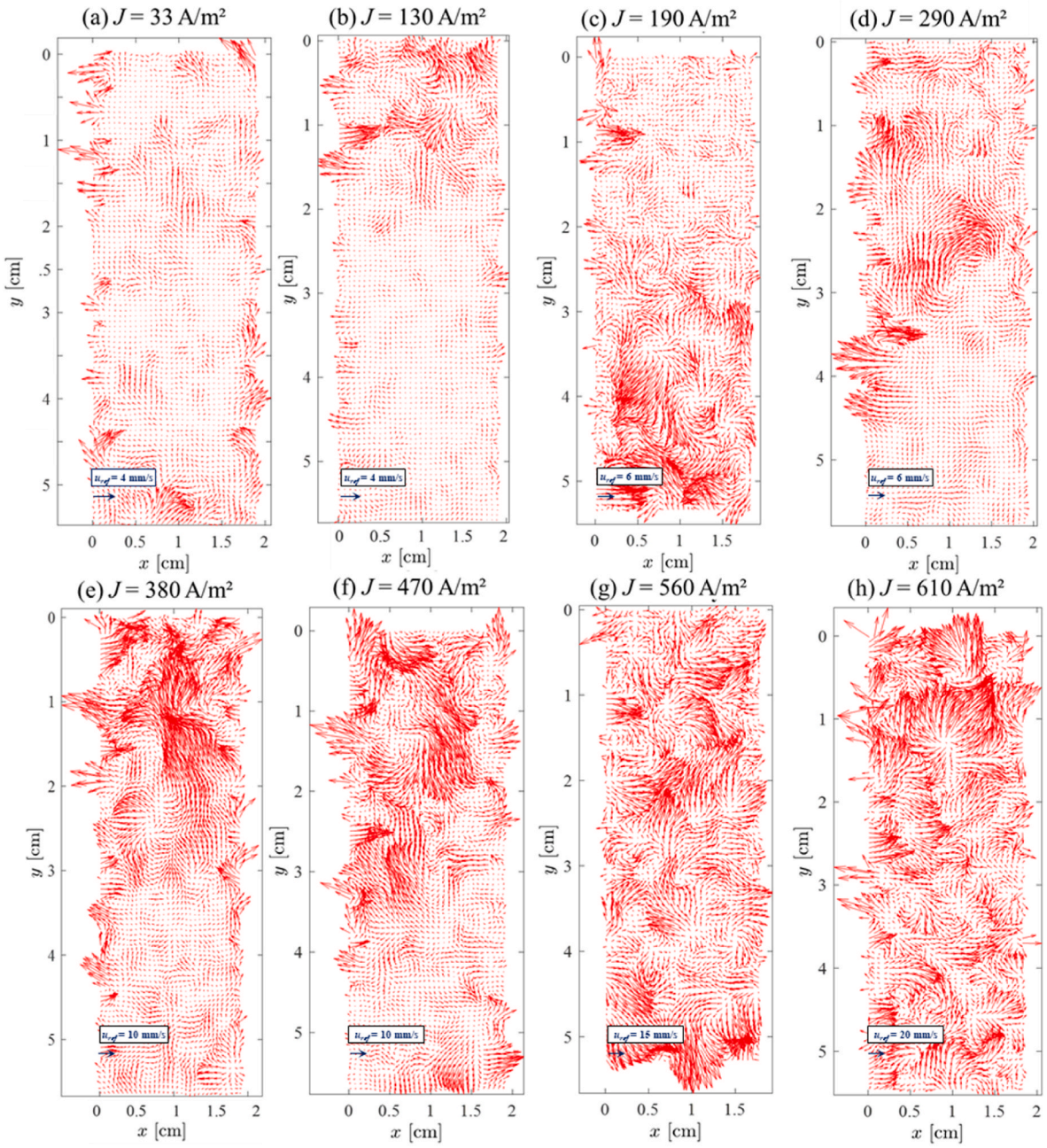

Fig. 6. Samples of velocity fields obtained from the optical flow method.

0 and $g\nabla \bullet \vec{U} = 0$, Eq. (3) simplifies the Horn-Schunck brightness constraint equation $\partial g/\partial t + \vec{U} \bullet \nabla g = 0$, according to Ref. [37].

In order to determine the optical flow, a variational formulation with a smoothness constraint is employed, based on a functional given by Eq. (4)

$$j(\boldsymbol{u}) = \int_{\Omega} \left\{ \left[\frac{\partial g}{\partial t} + \nabla \cdot \left(g\vec{U} \right) \right]^2 + \lambda \left(|\nabla u_x|^2 + |\nabla u_y|^2 \right) \right\} dxdy \tag{4}$$

where λ corresponds to the Lagrange multiplier, and Ω is an image domain. By minimizing Eq. (4), Euler-Lagrange equations obtained:

$$g\nabla \left[\frac{\partial g}{\partial t} + \nabla \cdot \left(g\vec{U} \right) - f \right] + \lambda \nabla^2 \vec{U} = 0 \tag{5}$$

The solution of Eq. (5) is found using the standard difference method with Neumann condition on the $\partial \vec{U}/\partial n = 0$ image domain.

In this study, tests were recorded with a high-speed camera MotionPro model Y4–S1, using 600 frames per second ($\Delta t = 1.67$ s), with a pixel size Δh of 67.2 μm. The data analysis of optical flow was performed using MATLAB™, using the open-source code provided by Ref. [38] and developed to estimate the instantaneous velocity field from sequential pairs of images.

2.2. Validation

This optical flow method was validated by Ref. [39], considering an error analysis by comparing its results with those of the robust PIV method. Relevant parameters, such as image intensity gradient magnitude, displacement magnitude, velocity magnitude, and velocity, were taken into account. However, to ensure the method's robustness for this study, bubble velocity analyses were conducted at various random points in the images, considering individual displacements and the time

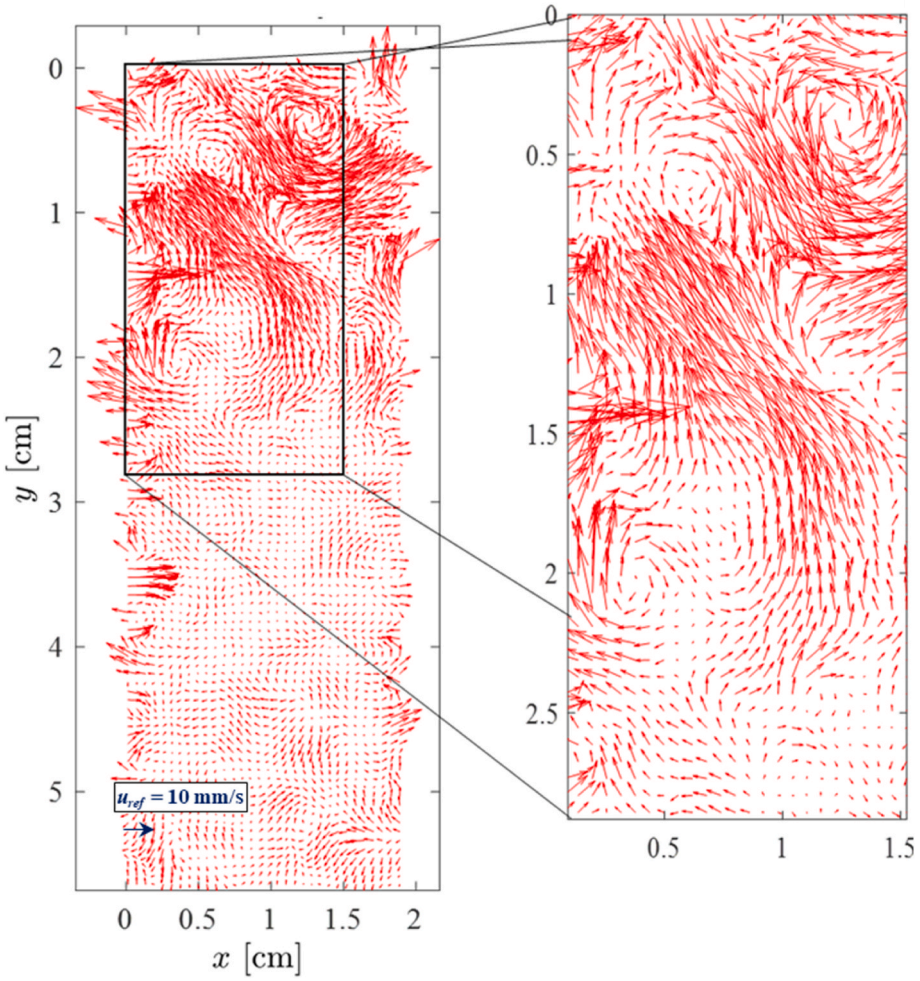

Fig. 7. Samples of small vorticities responsible for fluctuations of velocity components for $J = 320$ A/m^2.

interval between two images. In this analysis, bubbles larger than a certain threshold (denoted as Δh) were selected, and their vertical and horizontal velocities were compared with the velocities predicted by the optical flow.

Fig. 2 presents the results of individually analyzed velocities versus those obtained by the optical flow, with error margins of ±5%. In this sampling, the average errors were 3.09% and −0.98% for the x and y components, respectively. Assuming that variations in intensity throughout the image arise exclusively from the movement of bubbles and considering the fact that their motion is predominantly (though not exclusively) two-dimensional in the xy-plane, the mass conservation equation for the incompressible condition (*i.e.* $\nabla \bullet \vec{U} = 0$) can be a good indicator of the validity of the method employed for determining the velocity field. It is also important to emphasize that this assumption is grounded in the fact that the velocity field is obtained from a fixed time interval using a sequence of two images (instantaneous field) with no transient component of the mass conservation equation.

Fig. 3 presents the divergence of the velocity field for some analyzed cases. As can be observed, $\nabla \bullet \vec{U} = \mathscr{O}(10^{-3})$. Indeed, this difference may be related to the intrinsic error of the method itself, coupled with the loss of information associated with the orthogonal component of velocity that cannot be measured by the method.

Particularly, for cases with $J = 160$ A/m^2 and, especially, for $J = 440$ A/m^2, in some regions near the electrodes, an increase in the magnitude of the velocity divergence can be observed. This occurs due to the formation of more pronounced ripples in the rising bubble curtains.

3. Results

3.1. On flow pattern

During the electrolysis process, various bubble distributions arise due to fluid dynamics, as depicted in Fig. 4 for $J = 160$ A/m^2. Larger clusters of hydrogen bubbles are commonly observed at greater heights of the cathode (1). This occurrence is attributed to regions with higher vorticity near the electrolyte surface. At intermediate heights of the cathode (2), filament-like structures of hydrogen bubbles can be observed, primarily driven by buoyancy, resulting in a significant increase in the void fraction across the bubble coverage [5,18,40]. Smaller and more central dispersed bubbles are observed near the anode (3) for oxygen generation. The smallest bubbles, with greater dispersion, are generally noticed in more central regions between the electrodes (4). These patterns exhibit variations over time and within the electrolyte due to the turbulent nature of bubble dynamics. The current density variation, exemplified by Fig. 5, significantly influences both bubble generation and dynamics [41]. Hacha et al. [42] statistically investigated the influence of several parameters on the diameter of O_2 and H_2 bubbles during electroflotation. Their results indicate that most H_2 bubbles have diameters between 50 and 80 μm. In contrast, O_2 bubbles exhibit a wider range of average diameters, varying between 10 μm and 80 μm in most cases.

In contrast, O_2 bubbles exhibit a wider range of average diameters, varying between 10 and 80 μm in most cases. Similar values are also reported by Refs. [20,43]. Thus, the pixel size in this experiment

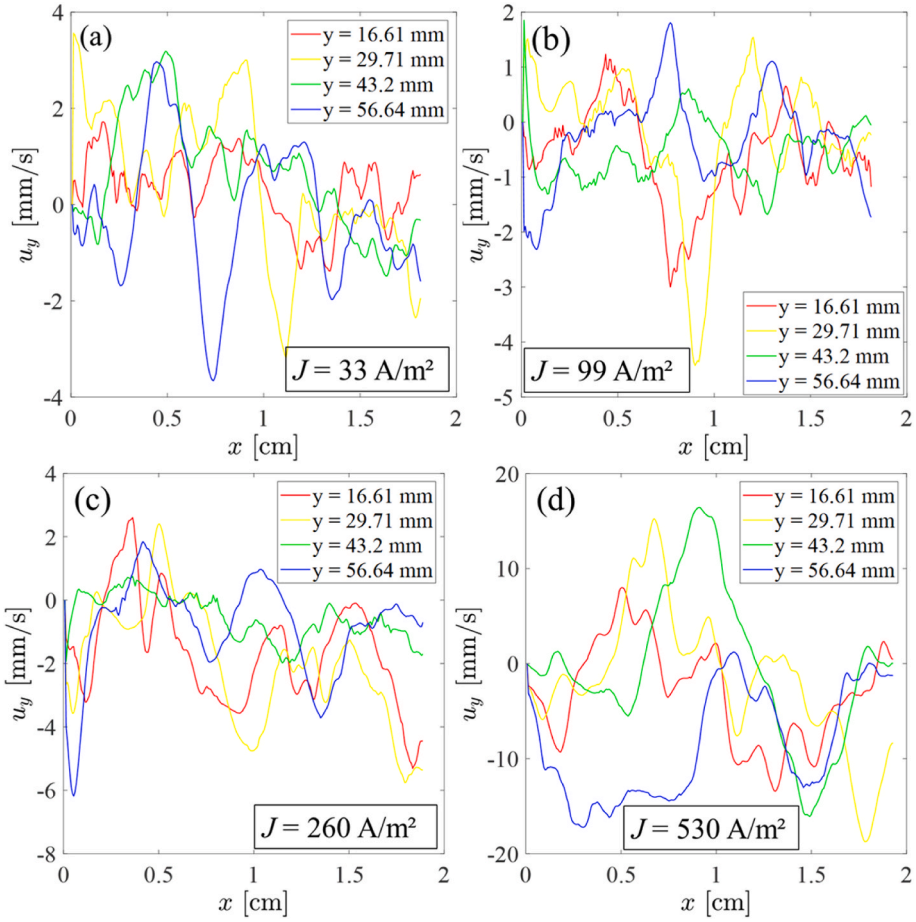

Fig. 8. Vertical velocity component for different depth levels from electrolyte surface.

corresponds to an intermediate value of bubble diameter found in experimental studies, especially in the case of H_2.

In Fig. 5, the dispersion of bubbles is evident, with both hydrogen and oxygen gases predominantly released through dispersed bubbles forming along the electrodes. The dispersion of bubbles in the electrolyte increases with the rise in current density. Under temporarily static conditions, larger bubbles can also be observed adhering to the electrodes. These bubbles form as smaller bubbles coalesce at distinct nucleation sites. As the current density increases, a higher concentration of bubbles near the electrolyte's surface is observed. This is primarily due to the bubbles encountering difficulties in overcoming the surface tension near the electrolyte's surface, resulting in the emergence of turbulent and recirculation zones between the electrodes.

3.2. *On the effect of current density on the velocity field*

Performing simultaneous measurements of fluid velocities and hydrogen bubble trajectories in electrolysis is a complex challenge. Although the optical flow cannot determine the velocities of the liquid phase, the velocities of the liquid-gas interface can be identified. It is crucial to emphasize that the velocities near the electrode surface play an essential role, as they significantly impact bubble detachment and the dynamics of the bubble layer.

The velocity field was obtained between the electrodes based on the sequential analysis of pairs of images using the optical flow method. Fig. 6 shows some samples of the fields obtained for different current densities. As expected, the increase in velocity field intensity depends on the increase in current density, exhibiting erratic behaviors associated with the increased turbulence of the electrolyte. For lower current densities (Fig. 6(a)–(b)), the velocity field predominantly exhibits a vertical pattern, although in some regions, vectors point in both directions relative to the electrode surface. These intermittencies are related to fluctuations in the bubble layer along the electrode walls. The heating of the electrodes and the electrolyte, caused by the Joule effect, also contributes to bubble dispersion [6].

For the case shown in Fig. 6(b), greater instabilities can be formed in the gap's upper region caused by H_2 and O_2 bubbles moving near the electrolyte surface. As the current density increases, these instability regions, dominated by recirculation zones, tend to spread between the electrodes (Fig. 6(c)–(h)). In these cases, there is an increase in velocity vectors throughout the gap, including the electrode surfaces, further enhanced by increased heating.

An example of recirculation zones can be observed in Fig. 7 for $J = 320$ A/m^2. In this case, these zones are predominant in the upper region of the electrolyte, close to its surface. For the region near the cathode, at a depth of approximately 2 cm, a vortex (clockwise) is observed, corresponding to the process of accelerating the bubble layer and wetting the electrode wall. On the other hand, two recirculation zones are observed in the range $0 \leq y \leq 1$ cm. In this case, two vortices with opposite directions are responsible for increasing the fluctuation of the bubble velocity field in regions farther from the electrode, making the release of bubbles from the electrolyte more challenging. In regions below a depth of 3 cm, small velocity gradients are observed near the electrodes, indicating the presence of low-intensity fluctuations in the bubble velocity fields. Similar dynamics were found by Ref. [44] during a study on water electrolysis using vertical electrodes spaced at 20 and 30 mm, also indicating velocity fluctuations along the electrodes with influence from the current density.

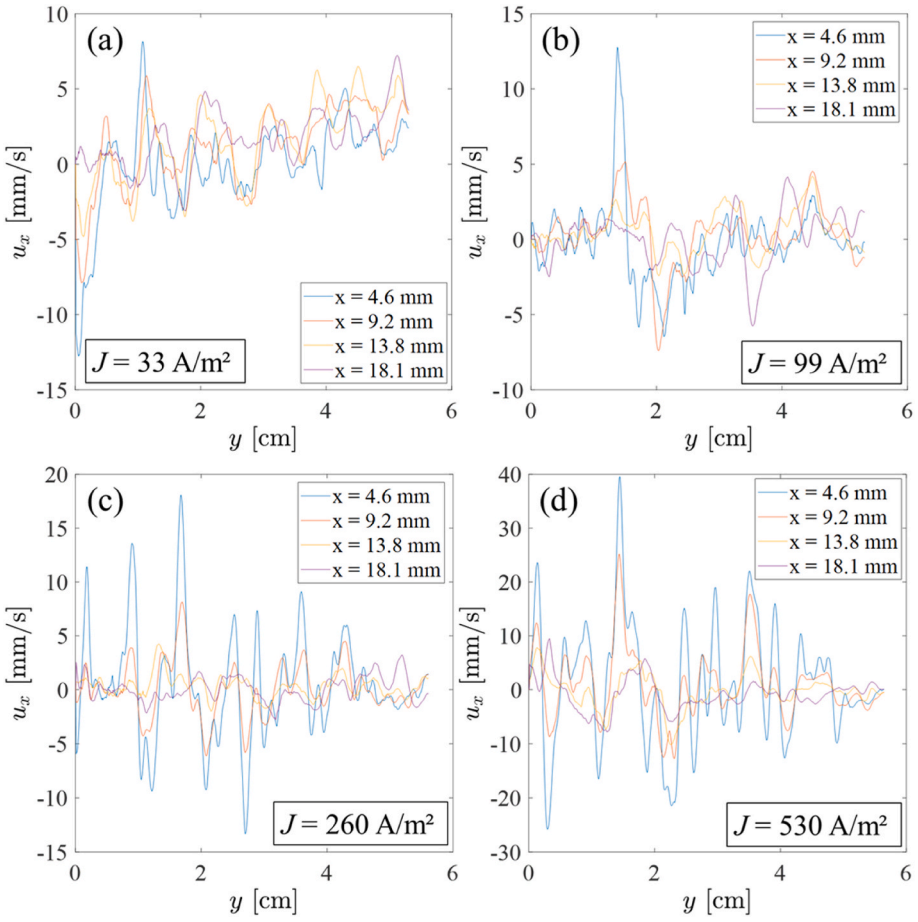

Fig. 9. Horizontal component of velocity for different sub-gaps.

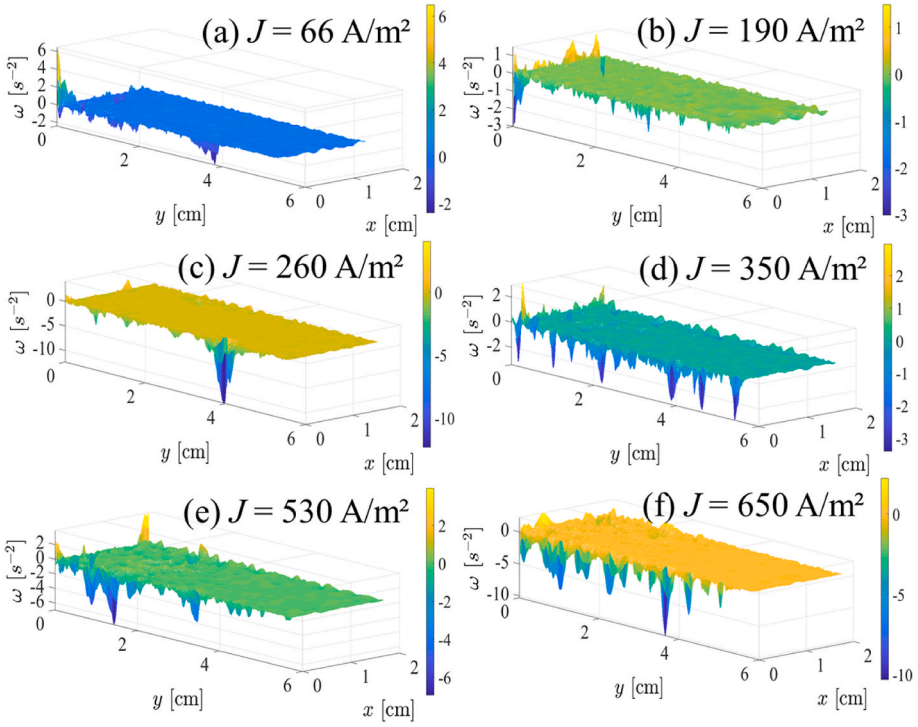

Fig. 10. Vorticity field obtained from velocity field for different conditions of *J*.

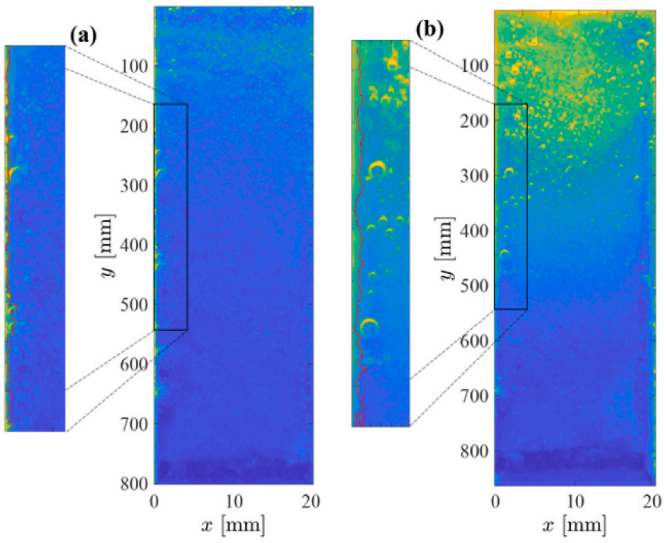

Fig. 11. Variation of the hydrogen plume thickness as a function of current density for J equal to (a) 99 A/m^2 and (b) 530 A/m^2.

3.3. On fluctuation of velocities

Fig. 8 presents the y-component of velocity (u_y) for different depth levels, considering the electrolyte surface. As observed, peaks of maximum velocity increase with higher current density, but such maximum intensities can be observed at different depths. This is due to the formation of circulation structures at different vertical positions between the electrodes. For $J \leq 99$ A/m^2, fluctuations in vertical velocity show higher frequencies for a depth of 16.61 mm, indicating greater intermittency in bubble velocity caused by zones containing small vortices. In fact, two distinct conditions can be observed along the gap. The first is related to rapid fluctuations in velocity without a change in direction (without the presence of negative velocities). In this case, the gas bubbles at this depth exhibit smooth oscillations caused by the positive components of vertical velocity along the vortices. The other condition involves rapid fluctuations, including negative vertical velocity. In this case, the bubbles undergo vertical oscillations caused by the swirling motion around the small vortices.

With increasing depths, oscillations with greater amplitudes are observed, indicating higher velocity intensities in both vertical component directions. For the case of $J = 33$ A/m^2, the oscillations can be greater than 4 mm/s at a depth of 56.64 mm and greater than 5 mm/s at a depth of 29.71 mm with $J = 99$ A/m^2. A greater homogeneity of vertical velocity oscillations is observed for the case of $J = 260$ A/m^2, although the amplitudes can reach values greater than 8 mm/s.

While buoyancy effects are predominant for bubble motion, analyzing their dynamics in the horizontal direction along the flow becomes relevant since the momentum transport in this direction occurs. Fig. 9 shows the horizontal velocity fluctuation for different gap widths. In all situations, the transitions of the horizontal velocity component $\partial u_x/\partial y$ occur more rapidly along the electrolyte depth. For the case of $J = 33$ A/m^2, in addition to the observed fluctuations, there is an increase in the average velocity (u_x) with respect to the electrolyte depth. This is due to the increase in recirculation zones near the electrolyte surface, although velocity peaks can be observed for $y < 2$ mm. For $J \geq 99$ A/m^2, the velocity peaks are more intense and tend to propagate throughout the electrolyte depth, especially for the sub-gap of 4.6 mm. However, for all cases, at depths $y \gtrsim 5$ mm, the fluctuations tend to attenuate due to the limited presence of bubbles formed from the electrodes. Similar structures have been reported by Refs. [20,45] based on velocity fields obtained from instantaneous images using different electrolytes.

Samples of the evolution of vorticity field intensity with increasing current density are presented in Fig. 10. As observed, the highest

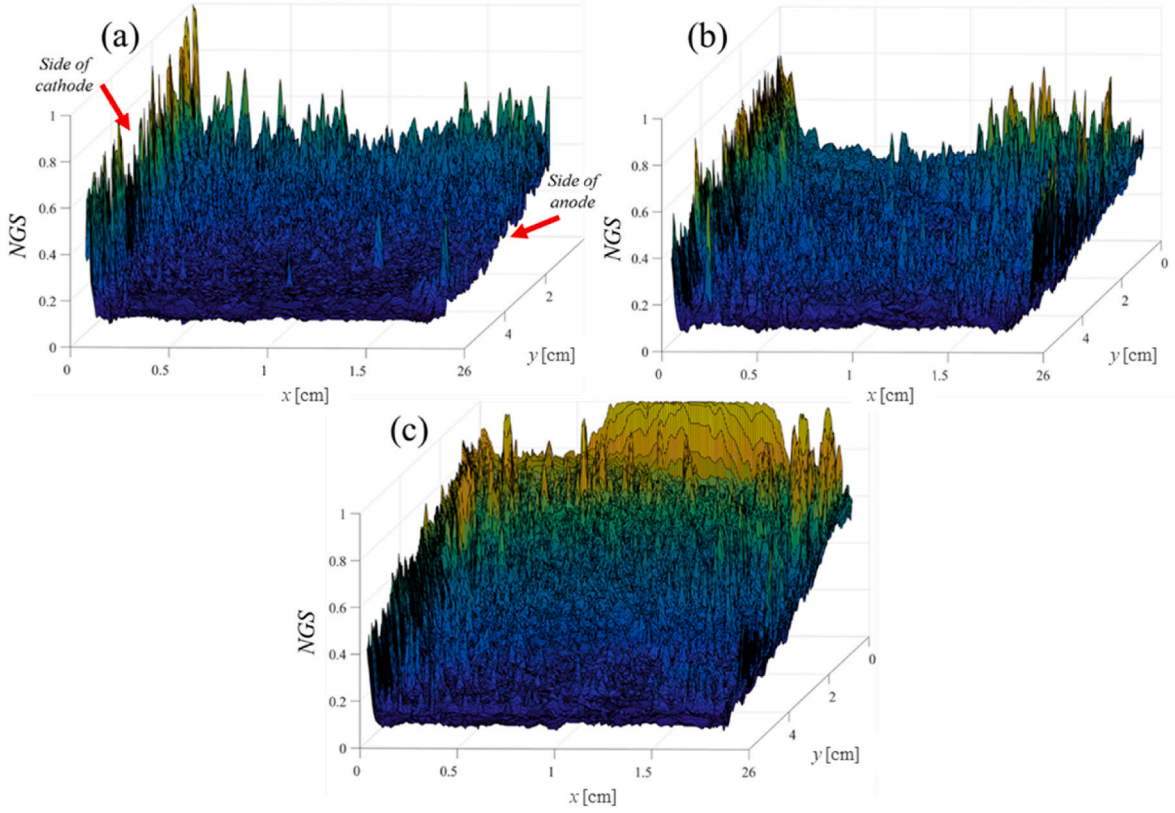

Fig. 12. Normalized intensity of grayscale for J: (a) 66 A/m^2; (b) 320 A/m^2 and (c) 610 A/m^2.

vorticity intensities are presented along the cathode, for different conditions of J, near the electrolyte surface. With the increase in current density, fluctuations in vorticity zones are also found in the upper region of the electrolyte, between the electrodes. In all cases, vorticity intensities vary between negative and positive values, indicating the presence of flows and counterflows responsible for the fluctuations in the velocity field, even in regions of greater depth in the cathode. The increase in vorticity intensity near the electrodes is directly related to the hydrogen and oxygen bubble layer fluctuations. The dynamics of the bubbles can be partly observed through the intensity of vorticity. In this case, swirls are generated in both directions of the z direction, caused by the vorticity. Thus, as shown in Fig. 10, the current density increase enhances the velocity field's instability. This indicates momentum transfer in the direction perpendicular to the 2D plane. This assertion is also supported by the field shown in Fig. 3. The uncertainty of vorticity is directly related to the uncertainty of its respective velocity components u_x and u_y. In this study, the methodology developed by Ref. [46] was implemented, considering the algorithm related to vorticity. In other words, its value is proportional to $\left((\partial u_y/\partial x)^2 dx^2 + (-\partial u_x/\partial y)^2 dy^2\right)^{1/2}$, and as $dx = dy = dh$, the uncertainty calculated from the vorticity fields varies between $\pm 1.6 \times 10^{-3}$ s^{-1}.

Several studies focused on the numerical simulation of hydrogen generation through electrolysis have presented the bubble layer with relatively well-defined thickness, not indicating the presence of fluctuations at its interfaces [4,17,25,27]. The absence of fluctuations may be possibly related to the limitation of numerical modeling, which does not predict instabilities at the interface caused by the difference in velocity between phases (e.g., Kelvin-Helmholtz instabilities). Another factor may be related to the increase in the electrode wall temperature. In fact, Oliveira et al. [47] observed an increase in the cathode wall temperature with the increase in current density during water electrolysis. With the increase in current density, more bubbles tend to increase the void fraction thickness along the electrode. Two samples indicating the variation in the thickness of the H_2 bubble layer near the cathode are presented in Fig. 11. In this case, a method was used for generating artificial colors based on different intensity levels of grayscale to aid in the visualization of the void fraction along the cathode. As observed, in addition to the increase in plume thickness with the increase in current density, there is an increase in velocity field fluctuations. It is also possible to observe the increase in void fraction near the upper part of the electrolyte, close to its surface. Based on the bubble layers identified by the frames in Fig. 11, their average thickness varies between 0.33 mm and 0.47 mm for $J = 99$ and 530 A/m^2, respectively. However, local fluctuations in these thicknesses can vary by $\pm$ 80% in some cases.

An estimate of the void fraction in the electrolyte can be derived from the analysis of normalized grayscale [48]. Fig. 12 illustrates the normalized grayscale (*NGS*) influenced by varying current densities. While bubble generation is contingent on the quantity of charge transferred, directly linked to current density, void fraction variations are associated with bubbles' dynamic behavior over time. Moreover, Faraday's law can elucidate the magnitude of departure velocity in the normal direction of bubble movement. A larger current density imparts momentum to the bubble in the normal direction of the electrode surface. Higher concentrations of the void fraction can be observed along the electrode (peaks) and in specific regions of the electrolyte. Variations in the height of each peak are related to different thicknesses of the bubble layer and the dispersion of gas within the layer.

4. Conclusion

This study investigated the hydrodynamic behavior and mass transfer performance in water electrolysis, focusing on the convective mass transfer phenomenon during hydrogen generation. By employing an optical flow method to analyze the velocity field of hydrogen bubbles, the research provided valuable insights into the dynamics of bubble behavior within the electrolyzer, enhancing the understanding of hydrogen generation through water electrolysis.

The experimental results revealed complex flow patterns influenced by buoyancy effects and current density variations. Two asymmetric flow patterns were observed, primarily driven by the buoyancy of hydrogen and oxygen bubble layers, resulting in increased turbulence within the electrolyte, especially in regions with lower depths. At higher current densities, the expansion of turbulent zones led to a decrease in the average velocity, while greater instabilities and recirculation zones occurred between the electrodes.

The findings highlighted the significant impact of current density variation on bubble generation, dispersion, and dynamics. Higher current densities resulted in larger clusters of hydrogen bubbles at greater heights of the cathode and increased dispersion of bubbles in the electrolyte. Moreover, the study elucidated the correlation between current density and velocity field intensity, with increased turbulence and instabilities observed with higher current densities.

The analysis of velocity fluctuations provided insights into the dynamic behavior of bubbles, revealing fluctuations in both vertical and horizontal velocity components, particularly in regions with small vortices and recirculation zones. These fluctuations were found to increase with higher current densities, indicating a more complex flow behavior influenced by bubble dynamics and momentum transfer.

Overall, this study contributes to the fundamental understanding of convective mass transfer in hydrogen generation through water electrolysis. The insights gained into the hydrodynamic behavior and mass transfer performance have implications for optimizing electrolyzer design and operational parameters to enhance hydrogen production efficiency. By elucidating the complex interactions between flow patterns, bubble dynamics, and current density variations, this research lays the foundation for further advancements in electrolysis technology for sustainable hydrogen production.

CRediT authorship contribution statement

Jeferson Diehl de Oliveira: Writing – review & editing, Writing – original draft, Validation, Supervision, Methodology, Investigation, Formal analysis, Conceptualization. **Elaine Maria Cardoso:** Writing – original draft, Supervision, Methodology, Formal analysis. **Reinaldo Rodrigues de Souza:** Writing – original draft, Methodology, Formal analysis. **Jacqueline Biancon Copetti:** Writing – original draft, Methodology, Formal analysis. **Lina Maria Varón:** Writing – original draft, Methodology, Formal analysis. **José Roberto Simões Moreira:** Writing – original draft, Methodology, Investigation.

Declaration of competing interest

The authors declare that they have no known competing financial interests or personal relationships that could have appeared to influence the work reported in this paper.

Acknowledges

We gratefully acknowledge the support of the RCGI – Research Centre for Greenhouse Gas Innovation (Cod. ANP 23.697-6/Cod. FUSP 403904), hosted by the University of São Paulo (USP) and sponsored by FUSP – University of são Paulo and Petronas, as well as the strategic importance of the support given by ANP (Brazil's National Oil, Natural Gas and Biofuels Agency) through the R&DI levy regulation.

References

[1] Nasser M, Megahed TF, Ookawara S, et al. A review of water electrolysis–based systems for hydrogen production using hybrid/solar/wind energy systems. Environ Sci Pollut Res 2022;29:86994–7018.

[2] Chien FS, Ngo QT, Hsu CC, et al. Assessing the capacity of renewable power production for green energy system: a way forward towards zero carbon electrification. Environ Sci Pollut Res 2021;28:65960–73.
[3] Ehrl A, Bauer G, Gravemeier V, Wall WA. A computational approach for the simulation of natural convection in electrochemical cells. J Comput Phys 2013;235:764–85.
[4] El-Askary WA, Sakr IM, Ibrahim KA, Balabel A. Hydrodynamics characteristics of hydrogen evolution process through electrolysis: numerical and experimental studies. Energy 2015;90(1):722–37.
[5] Schillings J, Doche O, Deseure J. Modeling of electrochemically generated bubbly flow under buoyancy-driven and forced convection. Int J Heat Mass Tran 2015;85:292–9.
[6] Hreiz R, Abdelouahed L, Fünfschilling D, Lapicque F. Electrogenerated bubbles induced convection in narrow vertical cells: PIV measurements and Euler – Lagrange CFD simulation. Chem Eng Sci 2015;134:138–52.
[7] Vogt H. The quantities affecting the bubble coverage of gas-evolving electrodes. Electrochim Acta 2017;235:495–9.
[8] Oliver P, Bourasseau C, Bouamama Pr B. Renew. Sustain. Energy Ver. 2017;78:280–300.
[9] Lohmann-Richters FP, Renz S, Lehnert W, Müller M, Carmo M. Review — challenges and opportunities for increased current density in alkaline electrolysis by increasing the operating temperature. J Electrochem Soc 2021;168:114501.
[10] Haug P, Kreitz B, Koj M, Turek T. Process modelling of an alkaline water electrolyzer. Int J Hydrogen Energy 2017;42(24):15689–707.
[11] Jones S, Evans G, Galvin K. Bubble nucleation from gas cavities – a review. Adv Colloid Interface Sci 1999;80:27–50.
[12] Van Damme S, Maciel P, Parys HV, Deconinck J, Hubin A, Deconinck H. Bubble nucleation algorithm for the simulation of gas evolving electrodes. Electrochem Commun 2010;12:664–7.
[13] Avci AC, Toklu E. A new analysis of two phase flow on hydrogen production from water electrolysis. Int J Hydrogen Energy 2022;47(11):6986–95.
[14] Ikeda H, Misumi R, Kojima Y, Haleem AA, Kuroda Y. Shigenori Mitsushima, Microscopic high-speed video observation of oxygen bubble generation behavior and effects of anode electrode shape on OER performance in alkaline water electrolysis. Int J Hydrogen Energy 2022;47(21):11116–27.
[15] Park H-K, Han J-W, Chung B-J. Influence of hydrodynamic parameters on the critical current density at water electrolysis: mass flux, channel inclination and inlet void fraction. Int J Hydrogen Energy 2022;47(12):7535–46.
[16] Su H, Sun J, Wang C, Wang H. Temperature impacts on the growth of hydrogen bubbles during ultrasonic vibration-enhanced hydrogen generation. Ultrason Sonochem 2024;102:106734.
[17] Abdelouahed L, Hreiz R, Poncin S, Valentin G, Lapicque F. Hydrodynamics of gas bubbles in the gap of lantern blade electrodes without forced flow of electrolyte: experiments and CFD modelling. Chem Eng Sci 2014;111:255–65.
[18] Zhu J, Zhang X, Lv P, Wang Y, Wang J. An experimental investigation of convective mass transfer characterization in two configurations of electrolyzers. Int J Hydrogen Energy 2018;43(18):8632–43.
[19] Babu R, Das MK. Experimental studies of natural convective mass transfer in a water-splitting system. Int J Hydrogen Energy 2019;44(29):14467–80.
[20] Chen Q, Lin W, Wang Z, Yu J, Li J, Wang Z. Flow field characterization between vertical plate electrodes in a bench-scale cell of electrochemical water softening. Water Sci Technol 2022;85(6):1736–53.
[21] Chandran P, Bakshi S, Chatterjee D. Study on the characteristics of hydrogen bubble formation and its transport during electrolysis of water. Chem Eng Sci 2015;138:99–109.
[22] Jianu OA, Rosen MA, Naterer GF, Wang Z. Two-phase bubble flow and convective mass transfer in water splitting processes. Int J Hydrogen Energy 2015;40:4047–55.
[23] Yang G, Yu S, Kang Z, Li Y, Bender G, Pivovar BS, Zhang F. Building electron/proton nanohighways for full utilization of water splitting catalysts. Adv Energy Mater 2020:1903871.
[24] Li Y, Yang G, Yu S, Mo J, Li K, Xie Z, Ding L, Wang W, Zhang F-Y. High-speed characterization of two-phase flow and bubble dynamics in titanium felt porous media for hydrogen production. Electrochim Acta 2021;370:137751.
[25] Torii K, Kodama M, Tokyo SH. Three-dimensional coupling numerical simulation of two-phase flow and electrochemical phenomena in alkaline water electrolysis. Int. J. J. Hydrogen Energy 2021;46:35088–101.
[26] Sarma SK, Singh A, Mohan R, Shukla A. Computational fluid dynamics simulation of bubble hydrodynamics in water splitting: effect of electrolyte inflow velocity and electrode morphology on cell performance. Int J Hydrogen Energy 2023;48:17769–82.
[27] Babay M-A, Adar M, Chebak A, Mabrouki M. Dynamics of gas generation in porous electrode alkaline electrolysis cells: an investigation and optimization using machine learning. Energies 2023;16:5365.
[28] Wosiak G, da Silva J, Sena SS, de Andrade RN, Pereira E. CFD simulation and experimental comparison of bubble-induced convection during electrochemical water splitting. Chem Eng J 2022;433(2):133194.
[29] Khalighi F, Deen NG, Tang Y, Vreman AW. Hydrogen bubble growth in alkaline water electrolysis: an immersed boundary simulation study. Chem Eng Sci 2023;267:118280.
[30] Sahore V, Kreidermacher A, Khan FZ, Fritsch I. Visualization and measurement of natural convection from electrochemically-generated density gradients at concentric microdisk and ring electrodes in a microfluidic system. J Electrochem Soc 2016;163(4):H3135.
[31] Sun D, Roth S, Black MJ. A quantitative analysis of current practices in optical flow estimation and the principles behind them. Int J Comput Vis 2014;106:115–37.
[32] Zhang C, Chen Z, Wang M, Li M, Jiang S. Robust non-local optical flow estimation with occlusion detection. IEEE Trans Image Process 2017;26:4055–67.
[33] Li R, Tan R, Cheong L. Robust optical flow estimation in rainy scenes. Proc. Eur. Conf. Comput. Vis.; 2017. p. 288–304.
[34] Mei L, Lai J, Xie X, Zhu J, Chen J. Illumination-invariance optical flow estimation using weighted regularization transform. IEEE Trans Circ Syst Video Technol 2019;30:495–508.
[35] Zhen C, Ge L, Chen Z, Li M, Liu W, Chen H. Refined TV-L optical flow estimation using joint filtering. IEEE Trans Multimed 2020;22:349–64.
[36] Liu T, Shen L. Fluid flow and optical flow. J Fluid Mech 2008;614:253–91.
[37] Horn BK, Schunck BG. Determining optical flow. Artif Intell 1981;17:185–204.
[38] Liu T. OpenOpticalFlow: an open source program for extraction of velocity fields from flow visualization images. J Open Res Software 2017;5(29):168.
[39] Liu T, Merat A, Makhmalbaf MHM, Fajardo C, Merati P. Comparison between optical flow and cross-correlation methods for extraction of velocity fields from particle images. Exp Fluid 2015;56:166–89.
[40] Sepahi F, Pande N, Chong KL, Mul G, Verzicco R, Lohse D, Mei BT, Krug D. The effect of buoyancy driven convection on the growth and dissolution of bubbles on electrodes. Electrochim Acta 2022;403:139616.
[41] Vogt H. Heat transfer in boiling and mass transfer in gas evolution at electrodes-The analogy and its limits. Int J Heat Mass Tran 2013;59:191–7.
[42] Hacha RR, Merma AG, Couto HJB, Torem ML. Measurement and analysis of H_2 and O_2 bubbles diameter produced by electroflotation processes in a modified Partridge-Smith cell. Powder Technol 2019;342:308–20.
[43] Jiménez C, Talavera B, Sáez C, Cañizares P, Rodrigo MA. Study of the production of hydrogen bubbles at low current densities for electroflotation processes. J Chem Technol Biotechnol 2010;85:1368–73.
[44] Weier T, Landgraf S. The two-phase flow at gas-evolving electrodes: bubble-driven and Lorentz-force-driven convection. Eur Phys J Spec Top 2013;220:313–22.
[45] Babu R, Das MK. Experimental studies of natural convective mass transfer in a water-splitting system. Int J Hydrogen Energy 2019;44(29):14467–80.
[46] Luff J, Drouillard T, Rompage A, et al. Experimental uncertainties associated with particle image velocimetry (PIV) based vorticity algorithms. Exp Fluid 1999;26:36–54.
[47] Oliveira JD, Woyciekoski ML, Leite TW, Cardoso EM, Copetti JB. Investigation on wall temperature fluctuation during hydrogen production by electrolysis. In: 27th international congress of mechanical engineering–COBEM; 2023. Florianópolis, Brazil.
[48] Lee JW, Sohn DK, Ko HS. Study on bubble visualization of gas-evolving electrolysis in forced convective electrolyte. Exp Fluid 2019;60:156.